G-2 Internal
Version 1.0
August 15, 2019

Performance study of the Cornell fast rotation Fourier analysis with toy Monte Carlo simulations

A. Chapelain[1], J. Fagin[1], D. Rubin[1], and D. Seleznev[1]

[1]Cornell University

Abstract

This note presents the performance study of the Cornell fast rotation Fourier analysis using toy Monte Carlo simulations.

Contents

1 Introduction

This note presents the performance study of the Cornell fast rotation Fourier analysis using toy Monte Carlo simulations. The goal of this work is to understand the performance and limitations of the Cornell fast rotation Fourier analysis using known signals. This work is important to understand the systematic limitation that will apply to actual experimental data. The details of the Cornell fast rotation Fourier method are presented in [1]. The user guide of the analysis code can be found here [2] and the toy Monte Carlo simulations here [3, 4].

The fast rotation Fourier method aims at reconstructing the radial distribution of the stored muon beam, via reconstructing the frequency distribution, in order to estimate the electric field correction to the anomalous spin precession frequency of the muon ω_a. The electric field correction C_E can be estimated in first approximation with the following formula:

$$C_E = \frac{\Delta\omega_a}{\omega_a} = -2n(1-n)\beta^2 \frac{\langle x_e^2 \rangle}{R_0^2}, \tag{1}$$

where

$$\langle x_e^2 \rangle = x_e^2 + \sigma^2, \tag{2}$$

where x_e is the equilibrium radius (average radial position) and σ the radial width of the beam, R_0 is the magic radius of 7112 mm, β the relativistic speed and, n the field index that relates to the electrostatic quadrupole electric field gradient like:

$$n = \frac{m\gamma r}{pB_0} \frac{\partial E_r}{\partial r}, \tag{3}$$

where m is the mass, γ the Lorentz factor, r the radial distance from the center of the storage ring, p the momentum, and E_r the radial component of the quadrupole electric field.

The goal for the Fermilab E–989 is an uncertainty budget on the electric field correction of 20 ppb. This uncertainty translates into knowing both the average and the with of the cyclotron revolution frequency distribution to couple 0.1 kHz, which corresponds to knowing both the equilibrium radius and the width of the radial distribution to couple 0.1 mm.

2 Toy Monte Carlo simulations

The fast rotation signal produced by the toy Monte Carlo is generated from two input distributions. The first one is the frequency distribution, which is equivalent to using the momentum distribution since the toy Monte Carlo simulates a pure weak focusing ring (frequency, radius and momentum are simply related via the storage magnetic field). The second one is the initial longitudinal beam profile. The only limitation of the simulated signals is the number of simulated muons, i.e., a statistical limitation. This limitation is very negligible due to the large size of the simulated samples. The generated fast rotation signal contains only the cyclotron motion of the beam. There is no built-in beam dynamics or anomalous spin precession effects. The generated beam has zero transverse emittance, i.e., the beam is point-like in the radial and vertical directions.

2.1 TMC #1: idealistic fast rotation signal

The toy Monte Carlo (TMC) #1 [3] is an idealistic fast rotation signal. The frequency (momentum, radial) distribution is a Gaussian distribution centered on the so-called "magic frequency" of 6,705 kHz with a width of 6 kHz (0.09%). The initial longitudinal beam profile is a Gaussian distribution with a width of 25 ns. Figure 1 shows the input frequency distribution as well as the input initial longitudinal beam profile. The generated fast rotation signal is shown in Fig. 2. The nominal time interval of the fast rotation signal is 1 ns.

2.2 TMC #3: data-like fast rotation signal

The toy Monte Carlo #3 [4] mimics the Run–1 data set. The frequency distribution is wide, asymmetric and its mean shifted to a lower frequency than the magic frequency, i.e., it corresponds to the beam being shifted radially outward. The initial longitudinal beam profile is the expected W-shape with a full length of 120 ns. Figure 3 shows the input frequency distribution as well as the input initial longitudinal beam profile. The generated fast rotation signal is shown in Fig. 4. The nominal time interval of the fast rotation signal is 1 ns.

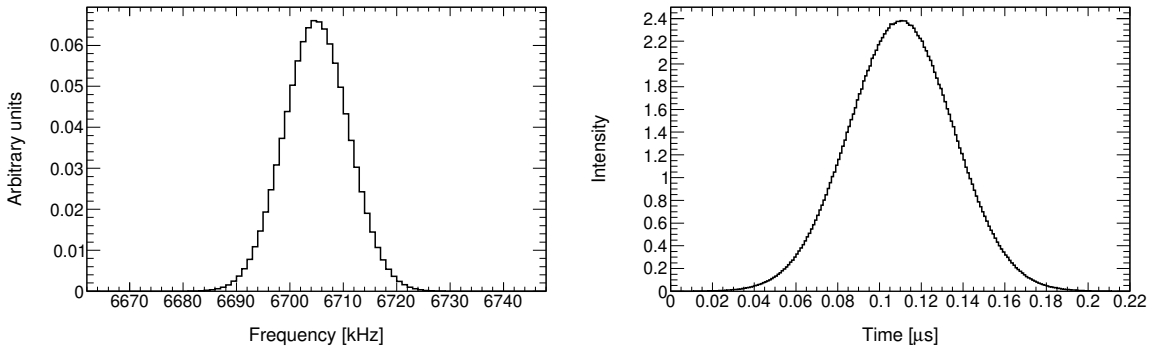

(a) (b)

Figure 1: TMC #1 input distributions: (a) Gaussian frequency distribution centered on 6,705 kHz with a width (one standard deviation) of 0.09% (6 kHz), (b) Gaussian initial longitudinal beam profile with a width (one standard deviation) of 25 ns. The frequency boundaries of (a) are set by the collimators aperture (6,662-6,747 kHz).

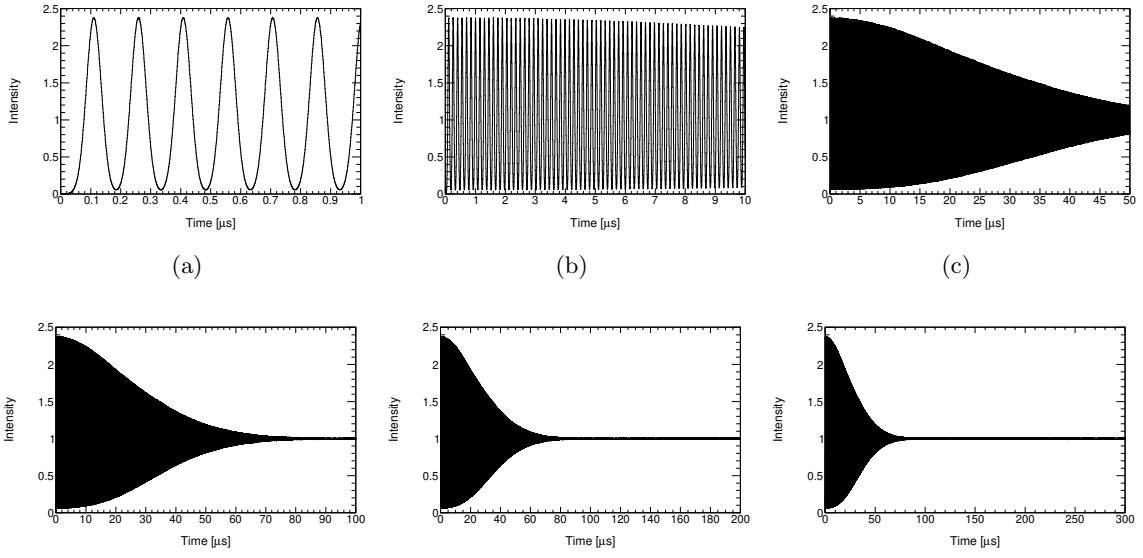

(a) (b) (c)

(d) (e) (f)

Figure 2: TMC #1 fast rotation signal for 6 time ranges: (a) 0-1, (b) 0-10, (c) 0-50, (d) 0-100, (e) 0-200, (f) 0-300 μs with respect to the beam injection. The time interval of the fast rotation signal is 1 ns.

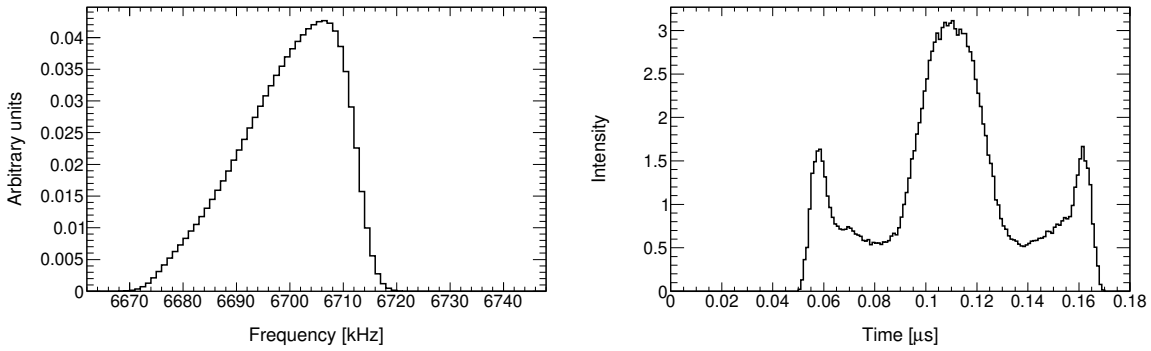

(a) (b)

Figure 3: TMC #3 input distributions: (a) asymmetric frequency distribution off-centered on 6,669 kHz with a width of 9 kHz, (b) W-shape initial longitudinal beam profile with a full length of 120 ns. The frequency boundaries of (a) are set by the collimators aperture (6,662-6,747 kHz).

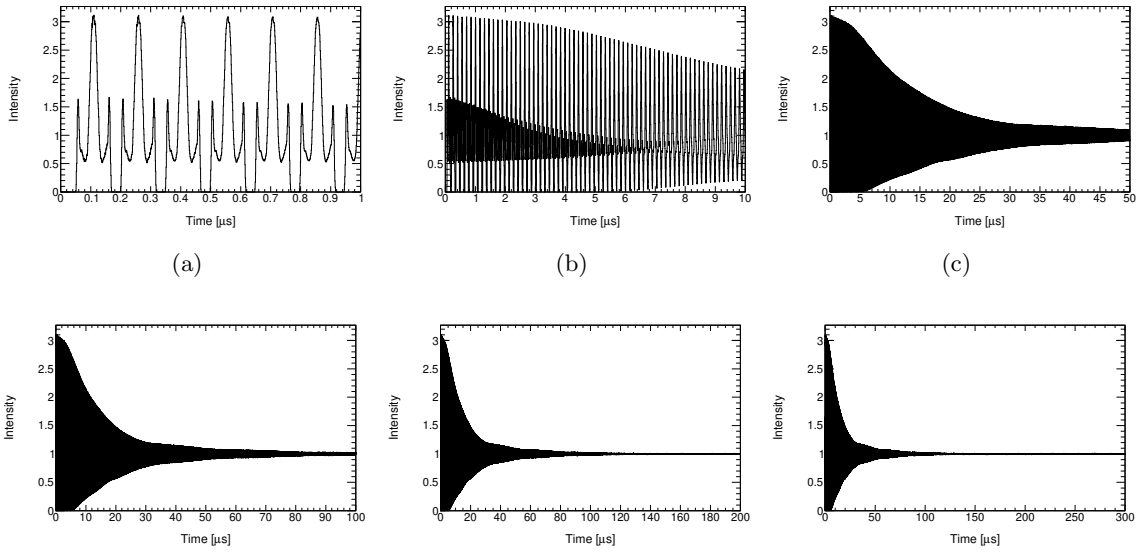

(a) (b) (c)

(d) (e) (f)

Figure 4: TMC #3 fast rotation signal for 6 time ranges: (a) 0-1, (b) 0-10, (c) 0-50, (d) 0-100, (e) 0-200, (f) 0-300 μs with respect to the beam injection. The time interval of the fast rotation signal is 1 ns.

3 Nominal analysis

This section will detail the nominal fast rotation Fourier analysis of the toy Monte Carlo simulations. The analysis procedure is presented in [1] and the reader is expected be familiar with the details before reading any further.

3.1 t_s and t_m optimization

The parameters t_s and t_m are chosen to match the values typically used to analyze Run–1 data set: t_s=4 μs, t_m=300 μs. These values are slightly optimized in order to have the intensities of the fast rotation signal at t_s and t_m to both be 1 in order to reduce the importance of spectral leakage (see [1] Sec. 7).

3.2 t_0 optimization

The t_0 optimization (see [1] Sec. 6) is performed within the nominal frequency range 6,630-6,780 kHz that includes physical and non-physical frequencies (outside the collimators aperture). The nominal number of iterations is 4 and the background fit function is a cardinal sine. Figure 5 and Fig. 6 show the results from the 4 iterations. The optimized t_0 value for the TMC #1 is 110.372 ns compared to the known value built-in the simulation (so-called "truth-level") of 110.376 ns, i.e., t_0 is mis-optimized by 4 ps. The optimized t_0 value for the TMC #3 is 109.958 ns compared to the known value in the simulation of 109.910 ns, i.e., t_0 is mis-optimized by 48 ps. The asymmetries in the TMC #3 simulation reduce slightly the performance of the method as expected. Section 4.1 will discuss the systematic bias on the fast rotation results due to a mis-optimized t_0 value.

3.3 Background correction

After optimizing t_s, t_m and t_0, the cosine Fourier transform can be corrected for the background (see [1] Sec. 5) as shown in Fig. 7 and in Fig. 8. The resulting frequency distributions are compared to the truth-level ones in Fig. 9. The difference in mean and width of the frequency distribution between the reconstructed-level and truth-level is at the 0.01 kHz level therefore an order of magnitude better than the desired goal.

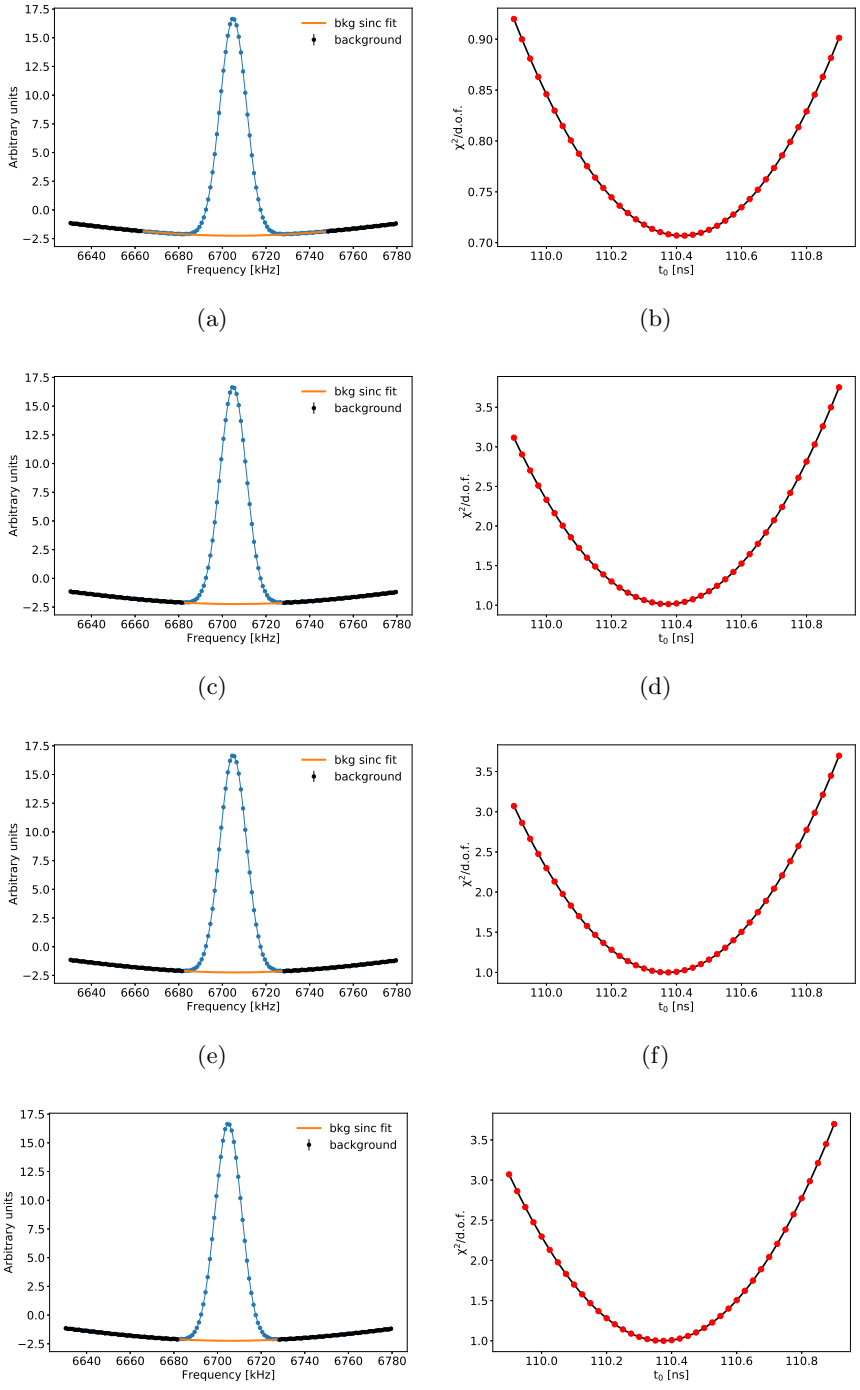

Figure 5: Results of the four iterations (from top to bottom) of the t_0 optimization procedure for the TMC #1 simulation. The figures on the left show the cosine Fourier transform with its cardinal sine background fit and the figures on the right show the χ^2 distribution of the background fit as a function of t_0 value. The optimized t_0 value is 110.372 ns compared to the known value built-in the simulation of 110.376 ns, i.e., t_0 is mis-optimized by 4 ps.

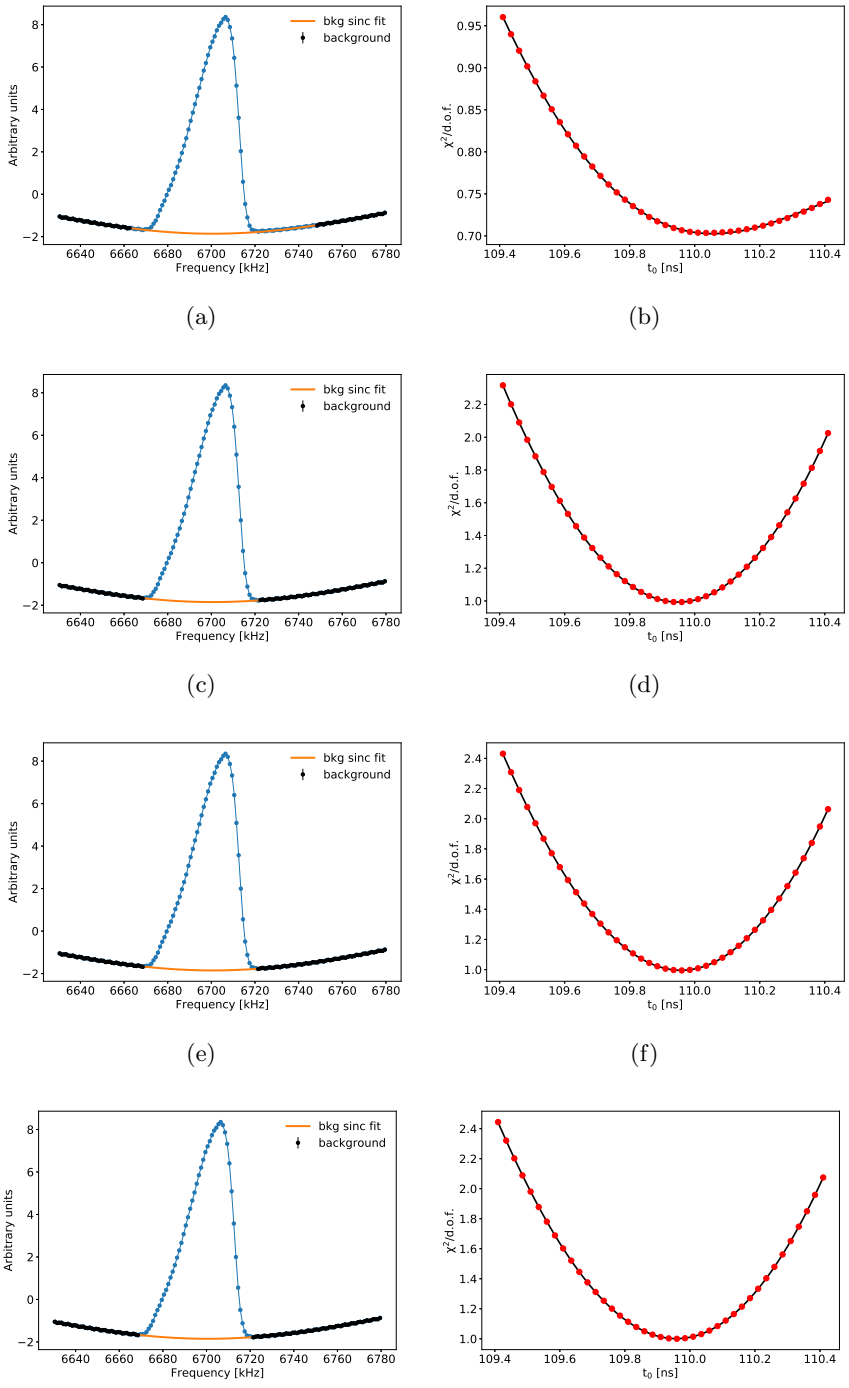

Figure 6: Results of the four iterations (from top to bottom) of the t_0 optimization procedure for the TMC #3 simulation. The figures on the left show the cosine Fourier transform with its cardinal sine background fit and the figures on the right show the χ^2 distribution of the background fit as a function of t_0 value. The optimized t_0 value is 109.958 ns compared to the known value in the simulation of 109.910 ns, i.e., t_0 is mis-optimized by 48 ps.

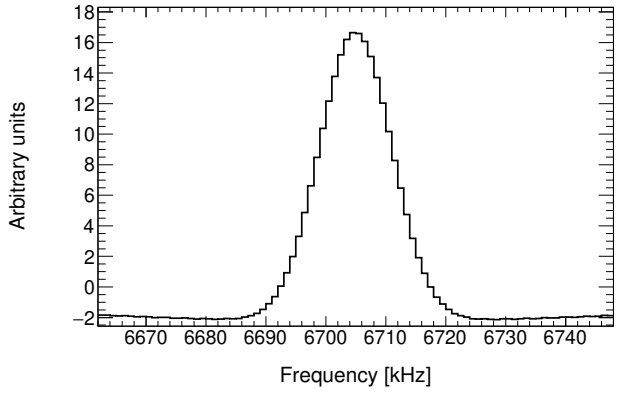

(a)

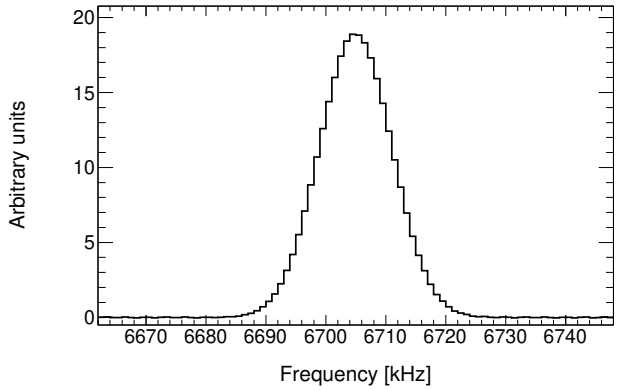

(b)

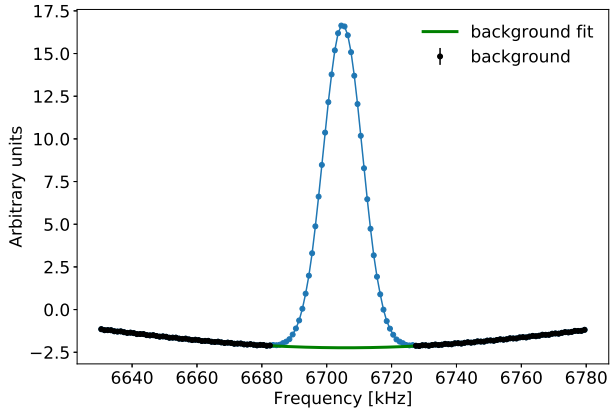

(c)

Figure 7: Fast rotation analysis frequency distribution outputs for the TMC #1: (a) cosine Fourier transform (frequency distribution before background correction), (b) corrected cosine Fourier transform (complete frequency distribution), and (c) cardinal sine fit to the background.

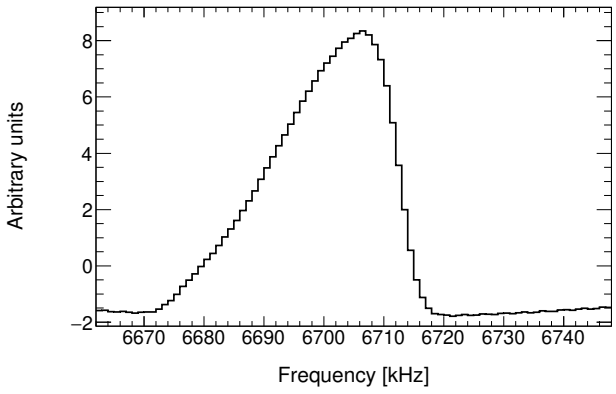

(a)

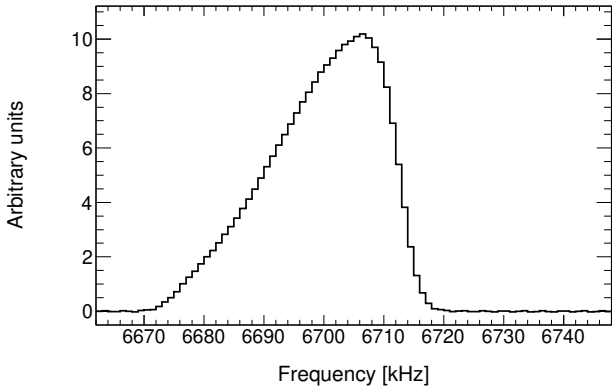

(b)

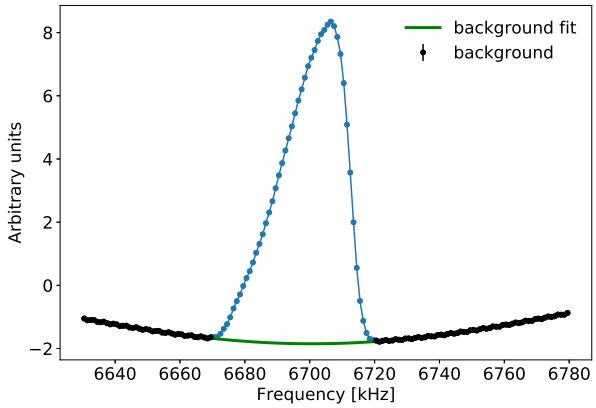

(c)

Figure 8: Fast rotation analysis frequency distribution outputs for the TMC #3: (a) cosine Fourier transform (frequency distribution before background correction), (b) corrected cosine Fourier transform (complete frequency distribution), and (c) cardinal sine fit to the background.

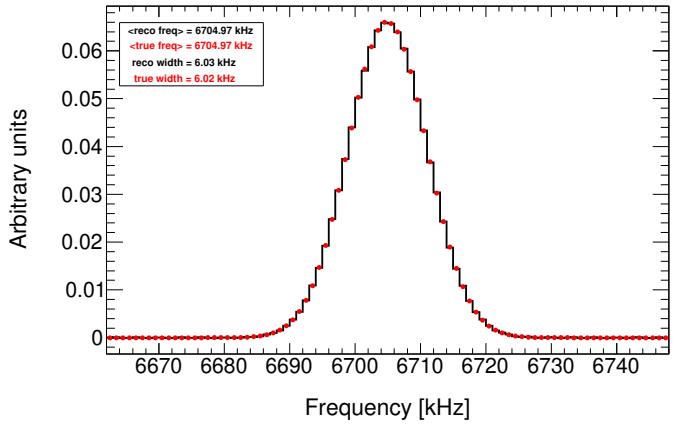

(a)

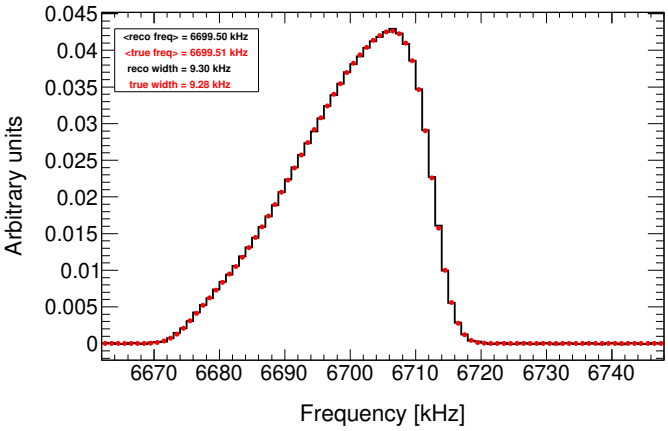

(b)

Figure 9: Comparison between the reconstructed- (black) and truth-level (red) frequency distributions for the (a) TMC #1 and (b) the TMC #3. The agreement is at the 0.01 kHz level therefore an order of magnitude better than the desired goal.

3.4 Radial distribution

The reconstructed frequency distributions can now be converted into their radial counterparts (see [1] Sec. 8). Figure 10 shows the reconstructed radial distributions overlaid with the truth-level ones. The reconstructed-level/truth-level differences in the frequency domain propagate to the radial domain. The systematic limitation of the method for these two Monte Carlo simulations is couple 0.01 mm. If one were to assume[1] a field index of n=0.108, the systematic limitation would be about 1 ppb on the electric field correction for both the TMC #1 and the TMC #3.

[1]The toy Monte Carlo simulates a pure weak focusing ring, thus without a field index.

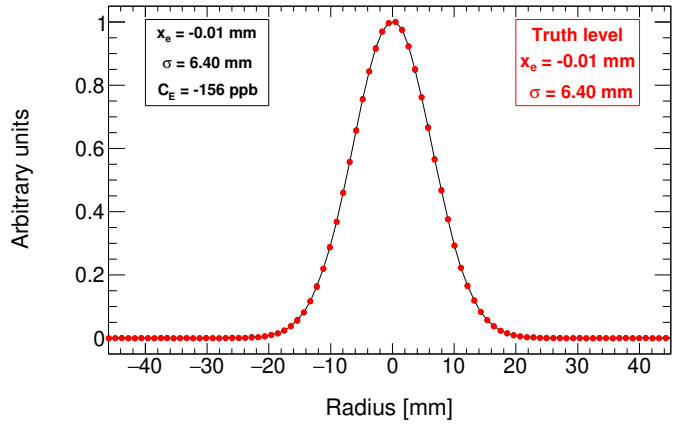

(a)

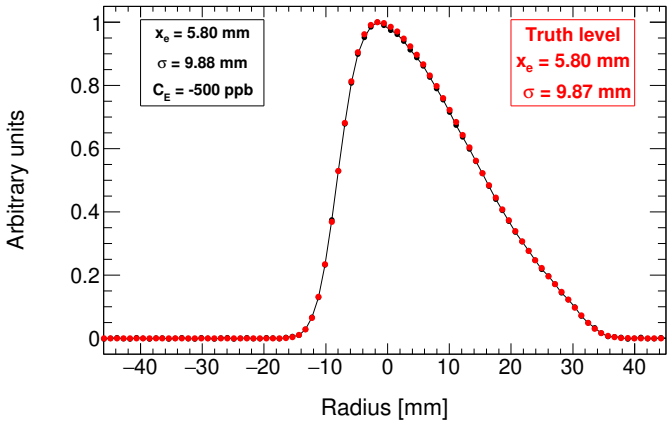

(b)

Figure 10: Comparison between the reconstructed- (black) and truth-level (red) radial distributions for the (a) TMC #1 and (b) the TMC #3. The agreement is at the 0.01 mm level therefore an order of magnitude better than the desired goal.

4 Systematic uncertainty studies

4.1 t_0 systematic

The sub-ns knowledge of the t_0 parameter is essential in order to reach the desired goal on the electric field correction C_E of 20 ppb, i.e., knowing both the equilibrium radius x_e and the width σ of the radial distribution to couple 0.1 mm.

Figure 11 shows how x_e, σ and C_E vary as a function of t_0 for the TMC #1. The equilibrium radius x_e varies by 0.8 mm over a 1 ns range. This seemingly unacceptable variation translates into a couple ppb shift in the electric correction value C_E. The reason is that the width varies little. Indeed, from eqs. (1) and (2), we see that x_e and σ contribute with the same weight to C_E. For the TMC #1, because of $\sigma = 6.40 >> x_e = -0.01$ mm, the width very largely dominates over x_e in the C_E calculation. Therefore C_E varies little over the 1 ns t_0 range.

Figure 12 shows how x_e, σ and C_E vary as a function of t_0 for the TMC #3. The equilibrium radius x_e and width σ vary respectively by 0.7 mm and 0.2 mm over a 1 ns range. This result in C_E varying by 50 ppb over the same range. It shows that for a radial distribution typical of the Run–1 data set, t_0 needs to be optimized better than 0.5 ns to yield an error on C_E below 20 ppb.

We have seen in Sec. 3.2 that t_0 is mis-optimized by about 50 ps for the TMC #3. Though not dramatic, this call for a systematic uncertainty estimation on t_0. One way to do it is to optimize t_0 using different background fit functions. Various functions can be used to reproduce the background for typical values of $t_s = 4$ μs[2] as presented in [5]: polynomial, cardinal sine, error function, triangle-based function. Tables 1 and 2 show the results of the t_0 optimization and fast rotation analysis using the various background fit functions.

It appears clearly that the cardinal sine, error and triangle-based functions perform the best. It is to be expected given the work detailed in [5]. The systematic uncertainty on the t_0 estimation for simulation and actual data will be taken as half the maximum variation in the results from these three functions. In the case of the TMC #1 and #3 it leads to a systematic uncertainty respectively of 0.5 ppb and 1.5 ppb on the electric field correction.

[2]For large t_s, the various functions do not perform equally. The best ones being the error function and the triangle-based function.

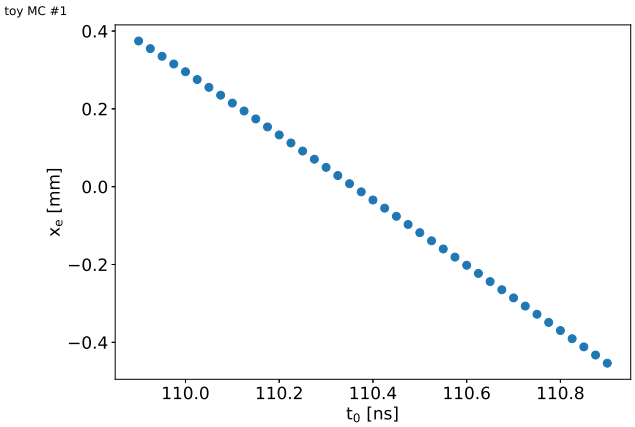

(a)

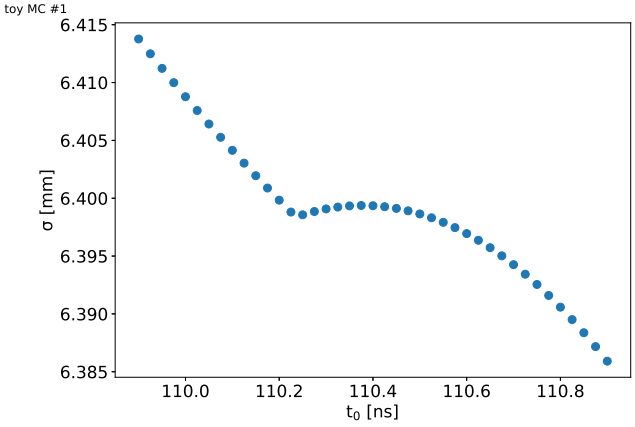

(b)

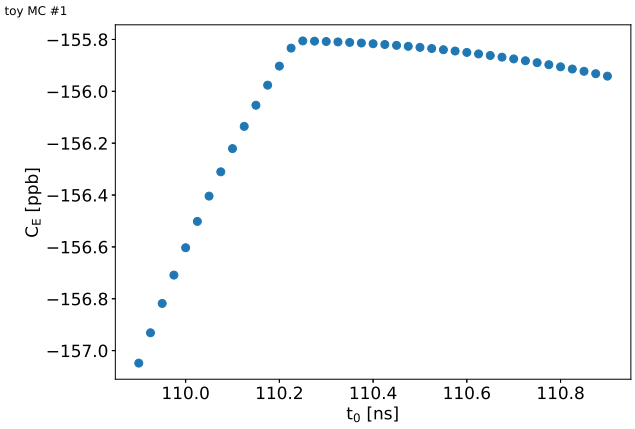

(c)

Figure 11: Results of the fast rotation analysis as a function of t_0 for a 1 ns range for the TMC #1: (a) equilibrium radius, (b) width, and (c) electric field correction C_E. The known answers are (a) $x_e = -0.01$, (b) $\sigma = 6.40$ mm, and (c) $C_E = -156$ ppb.

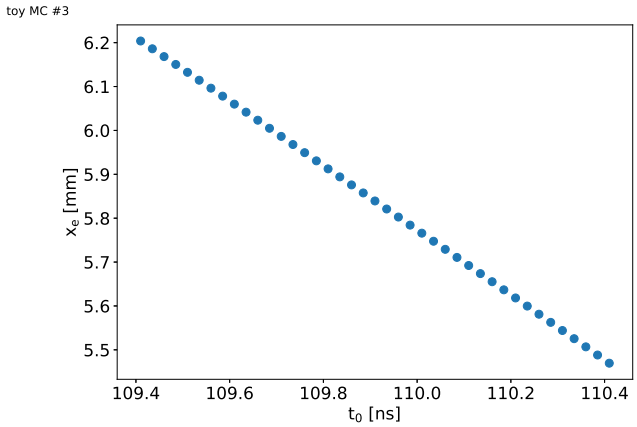

(a)

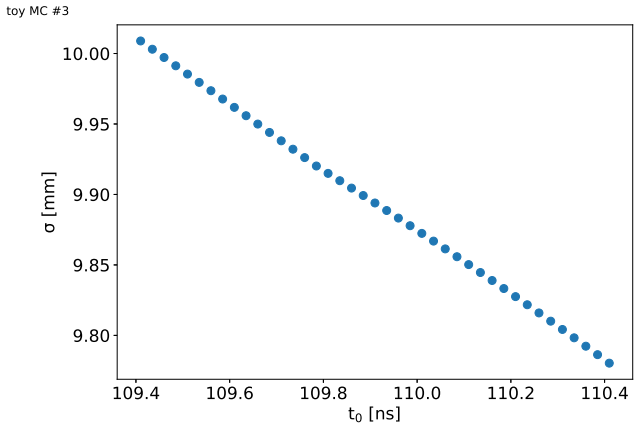

(b)

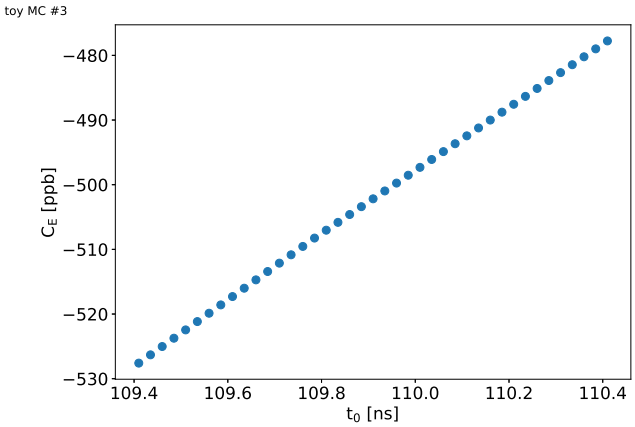

(c)

Figure 12: Results of the fast rotation analysis as a function of t_0 for a 1 ns range for the TMC #3: (a) equilibrium radius, (b) width, and (c) electric field correction C_E. The known answers are (a) $x_e = 5.80$, (b) $\sigma = 9.87$ mm, and (c) $C_E = -499$ ppb.

	t_0 [ns]	x_e [mm]	σ [mm]	C_E [ppb]
known answer	110.376	-0.01	6.40	-156
2nd order polynomial	110.388	-0.01	6.28	-150
3rd order polynomial	110.348	0.00	6.28	-150
cardinal sine	110.372	-0.01	6.40	-156
error function	110.372	-0.01	6.40	-156
triangle function	110.310	0.03	6.41	-156
systematic	0.031	0.02	0.01	0.5

Table 1: Estimation of the t_0 systematic uncertainty for the TMC #1. The systematic uncertainty is estimated as half the maximum difference between the following background fit functions: cardinal sine, error function, triangle-based function.

	t_0 [ns]	x_e [mm]	σ [mm]	C_E [ppb]
known answer	110.910	5.80	9.87	-499
2nd order polynomial	110.040	5.72	9.83	-492
3rd order polynomial	110.199	5.66	9.80	-487
cardinal sine	109.958	5.80	9.88	-500
error function	109.958	5.80	9.88	-500
triangle function	109.910	5.84	9.90	-503
systematic	0.024	0.02	0.01	1.5

Table 2: Estimation of the t_0 systematic uncertainty for the TMC #3. The systematic uncertainty is estimated as half the maximum difference between the following background fit functions: cardinal sine, error function, triangle-based function.

4.2 t_s systematic

In an ideal world, the fast rotation Fourier analysis would be performed from $t_s = t_0$ to avoid the complication due to missing early data. We know it is not possible for Run–1 data set as shown in [6, 7, 8, 9]. The ideal world would also allow to start the analysis at $t_s = 30$ μs, time at which the anomalous spin precession frequency analysis starts. The main reason for skipping the first 30 μs is to leave time for the beam to stabilize after the end of the scraping period around 25 μs. Thus, we would hope to show that the fast rotation results do not change between the earliest possible t_s and $t_s = 30$ μs. The TMC #1 and #3 have a frequency/radial distribution that is constant versus t_s. Performing a t_s scan test the stability of the method versus t_s. For the TMC #1, Fig. 13, 14, 15 show the results of the t_s scan fitting the background with respectively the error function, the triangle-based function and the cardinal sine. The error function is the expected exact form of the background [5], given the TMC #1 has Gaussian profiles, and therefore performs well up to 30 μs. The triangle-based function, that performs almost as well as the error function, is a more general form that allows asymmetry in the frequency distribution. The cardinal sine function is expected to fail at smaller t_s value because being a Taylor series approximation of the two other functions (the same way a polynomial fit would fail at even smaller t_s because being a Taylor series approximation of the cardinal sine function). The boundaries of the background fit is fixed for each function to the boundaries optimized at $t_s = 4$ μs. Not fixing the fit boundaries would yield discreet jumps in the results whenever the size of the background window varies (usually one or two data points are added or removed). The t_0 value being used is the optimized one for each function at $t_s = 4$ μs. The modulation of the results as a function of t_s (most visible in Fig. 13,) is likely due to a non-zero spectral leakage. The results at very early times for some of the functions appear as outliers due to the difficulty in fitting the almost flat background of the cosine Fourier transform (for very small t_s values the background is almost nonexistent). At very early times using a simple second polynomial fit yields better results. This is a "non-problem"[3] for Run–1 given the data is not usable before about 4 μs.

For the TMC #3, Fig. 16, 17, 18 show the results of the t_s scan for respectively fitting the background with the error function, the triangle-based function and the cardinal sine. Due to the asymmetric non-Gaussian nature of the frequency distribution, the triangle-based function shows the best performance. It performs within 10 ppb of the known answer up until 30 μs, which is very encouraging given this simulation mimics the Run–1 data. Figure 19 shows the background fit using the triangle-based function for six different t_s values and Fig. 20 the fit residuals and χ^2 per degrees of freedom. The systematic uncertainty in the data will be taken as half the maximum variation observed in the scan results using the triangle-based function with an upper bound of 25 μs. For instance Fig. 14 clearly shows

[3] We of course would prefer having access to $t_s = t_0$ to avoid the background correction complication.

that the performance diverges passed 25 μs.

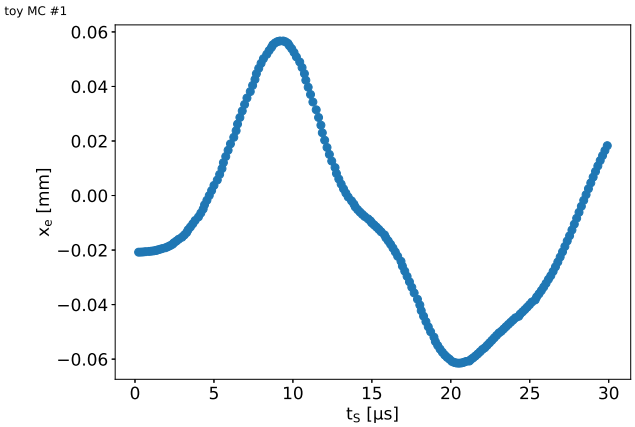

(a)

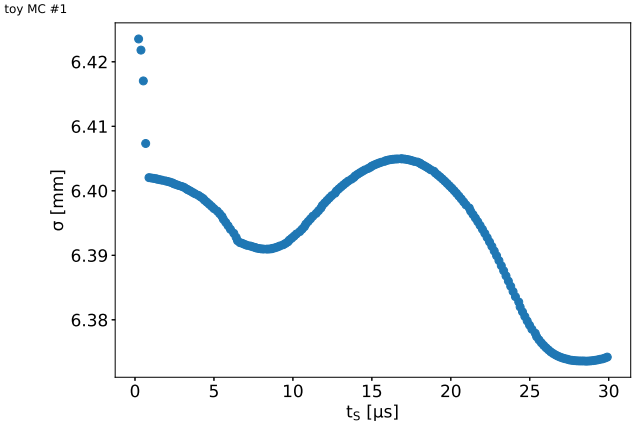

(b)

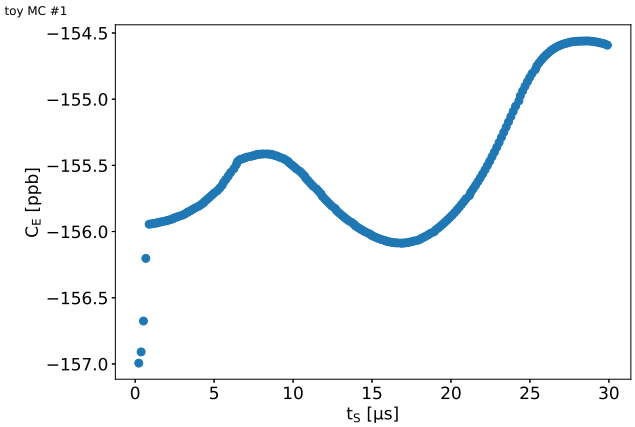

(c)

Figure 13: Results of the fast rotation analysis as a function of t_s for a 30 μs range of the TMC #1 using the error function background fit: (a) equilibrium radius, (b) width, and (c) electric field correction C_E. The known answers are: (a) $x_e = -0.01$ mm, (b) $\sigma = 6.40$ mm, and (c) $C_E = -156$ ppb.

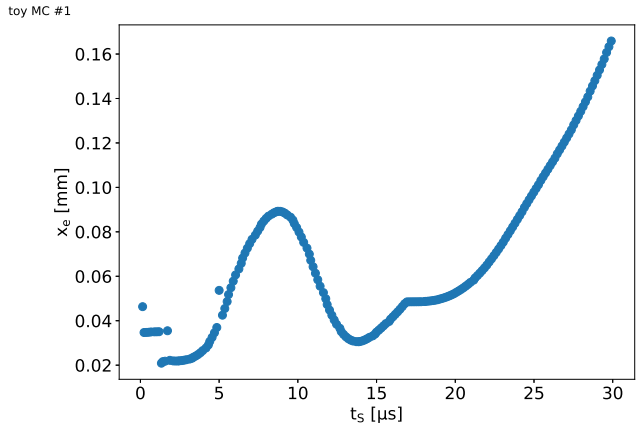

(a)

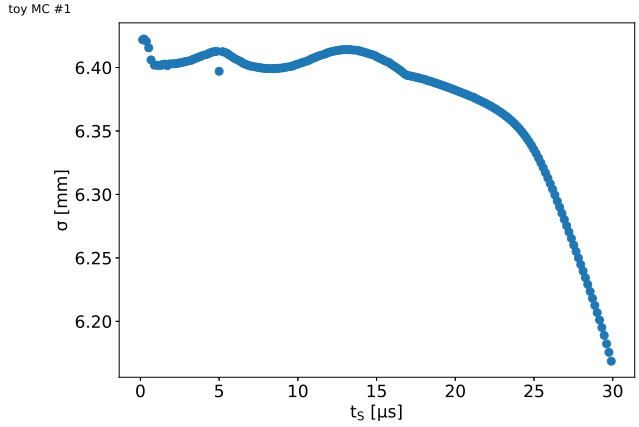

(b)

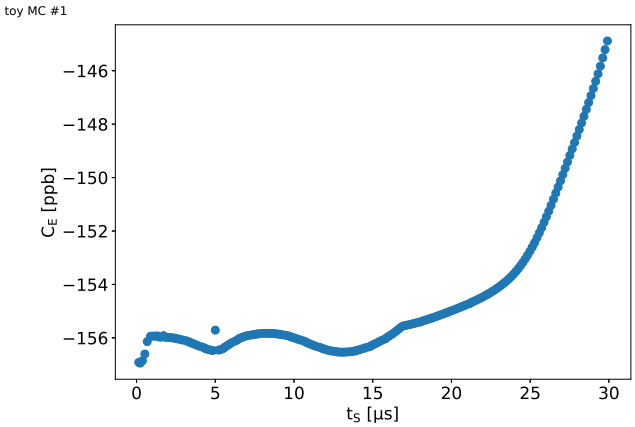

(c)

Figure 14: Results of the fast rotation analysis as a function of t_s for a 30 μs range of the TMC #1 using the triangle-based function background fit: (a) equilibrium radius, (b) width, and (c) electric field correction C_E. The known answers are: (a) $x_e = -0.01$ mm, (b) $\sigma = 6.40$ mm, and (c) $C_E = -156$ ppb.

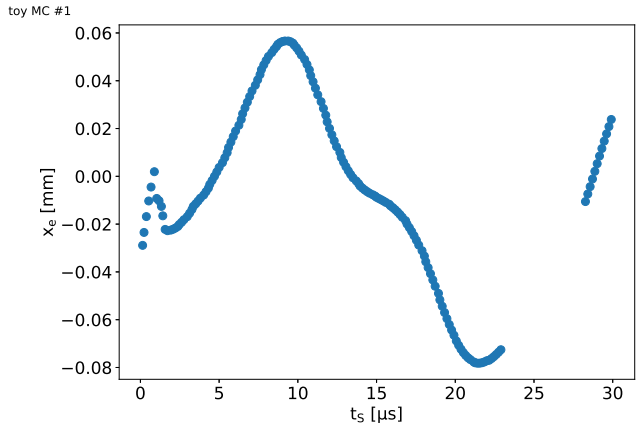

(a)

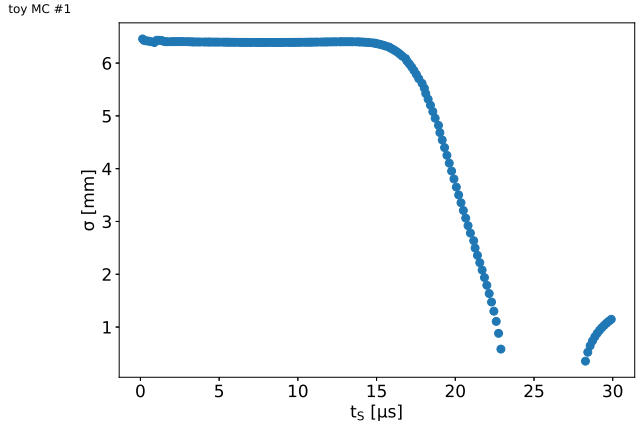

(b)

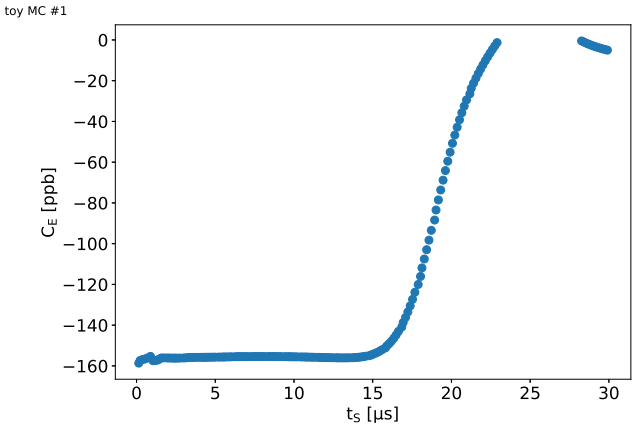

(c)

Figure 15: Results of the fast rotation analysis as a function of t_s for a 30 μs range of the TMC #1 using the cardinal sine function background fit: (a) equilibrium radius, (b) width, and (c) electric field correction C_E. The known answers are: (a) $x_e = -0.01$ mm, (b) $\sigma = 6.40$ mm, and (c) $C_E = -156$ ppb.

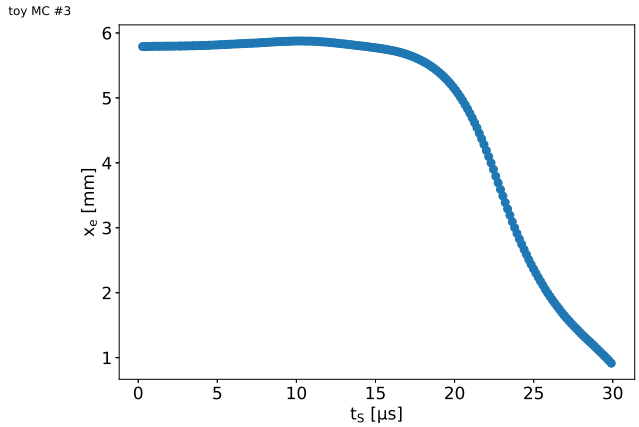

(a)

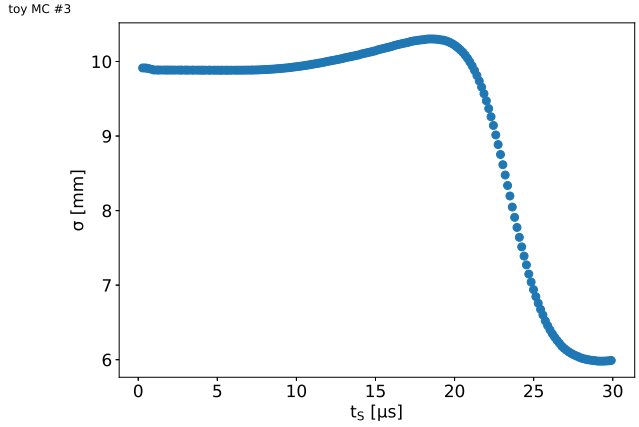

(b)

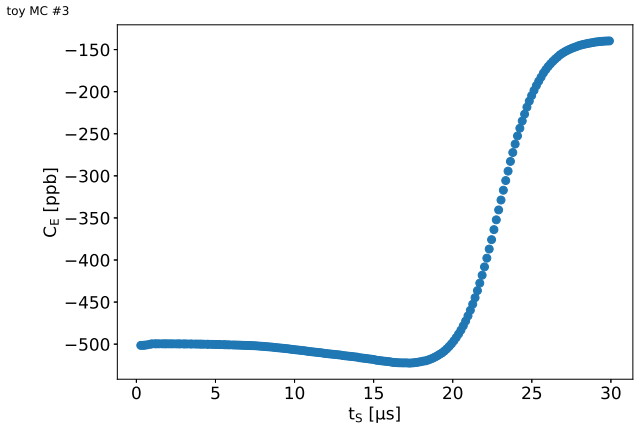

(c)

Figure 16: Results of the fast rotation analysis as a function of t_s for a 30 μs range for the TMC #3 using the error function background fit: (a) equilibrium radius, (b) width, and (c) electric field correction C_E. The known answers are: (a) $x_e = 5.80$ mm, (b) $\sigma = 9.87$ mm, and (c) $C_E = -499$ ppb.

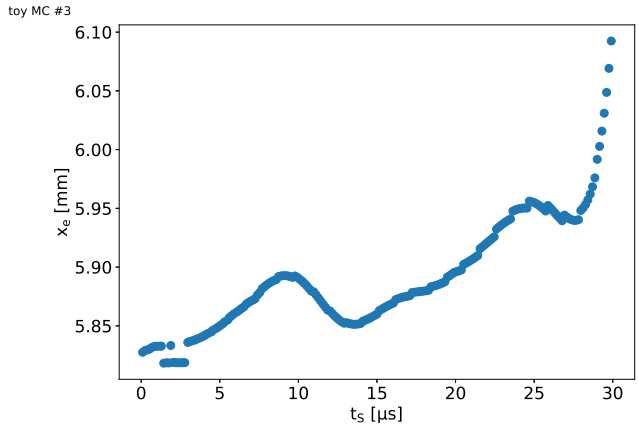

(a)

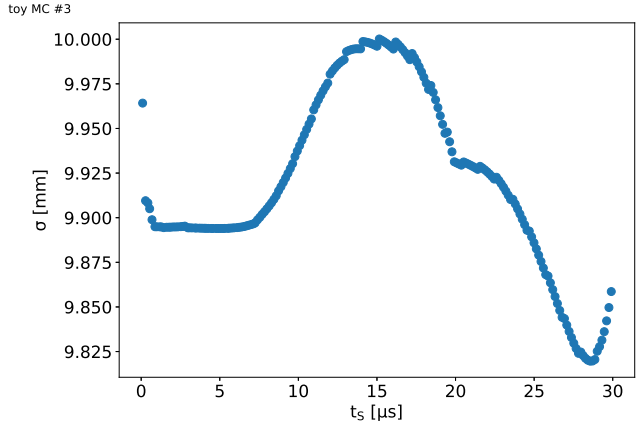

(b)

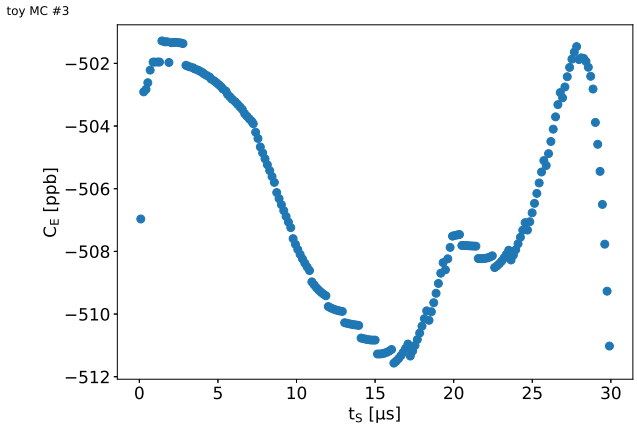

(c)

Figure 17: Results of the fast rotation analysis as a function of t_s for a 30 μs range for the TMC #3 using the triangle-based function background fit: (a) equilibrium radius, (b) width, and (c) electric field correction C_E. The known answers are: (a) $x_e = 5.80$ mm, (b) $\sigma = 9.87$ mm, and (c) $C_E = -499$ ppb.

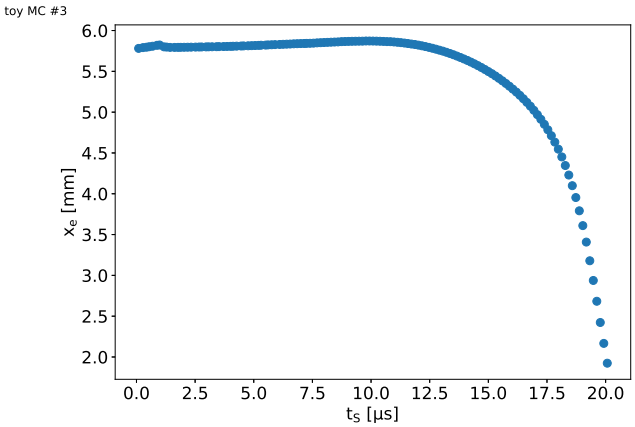

(a)

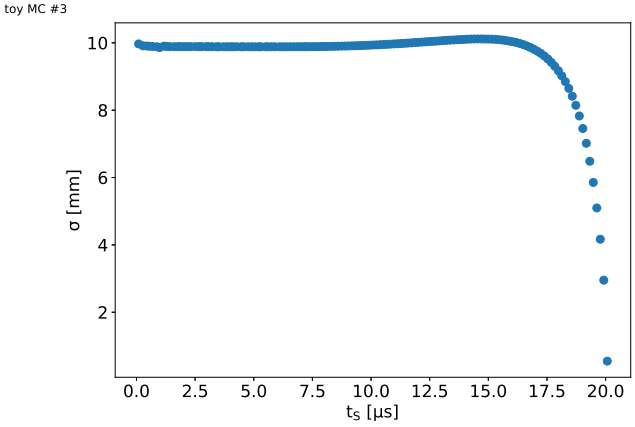

(b)

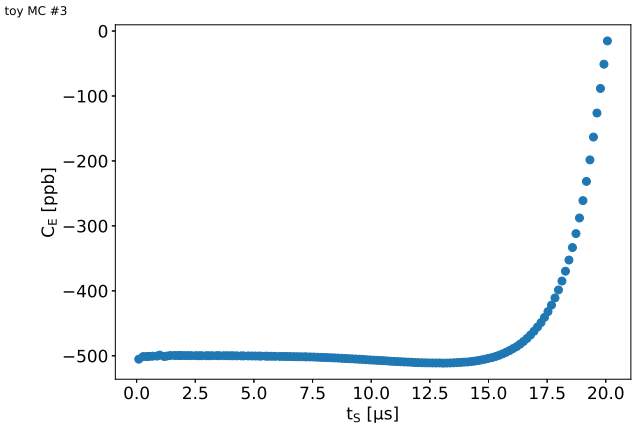

(c)

Figure 18: Results of the fast rotation analysis as a function of t_s for a 20 μs range for the TMC #3 using the cardinal sine function background fit: (a) equilibrium radius, (b) width, and (c) electric field correction C_E. The known answers are: (a) $x_e = 5.80$ mm, (b) $\sigma = 9.87$ mm, and (c) $C_E = -499$ ppb.

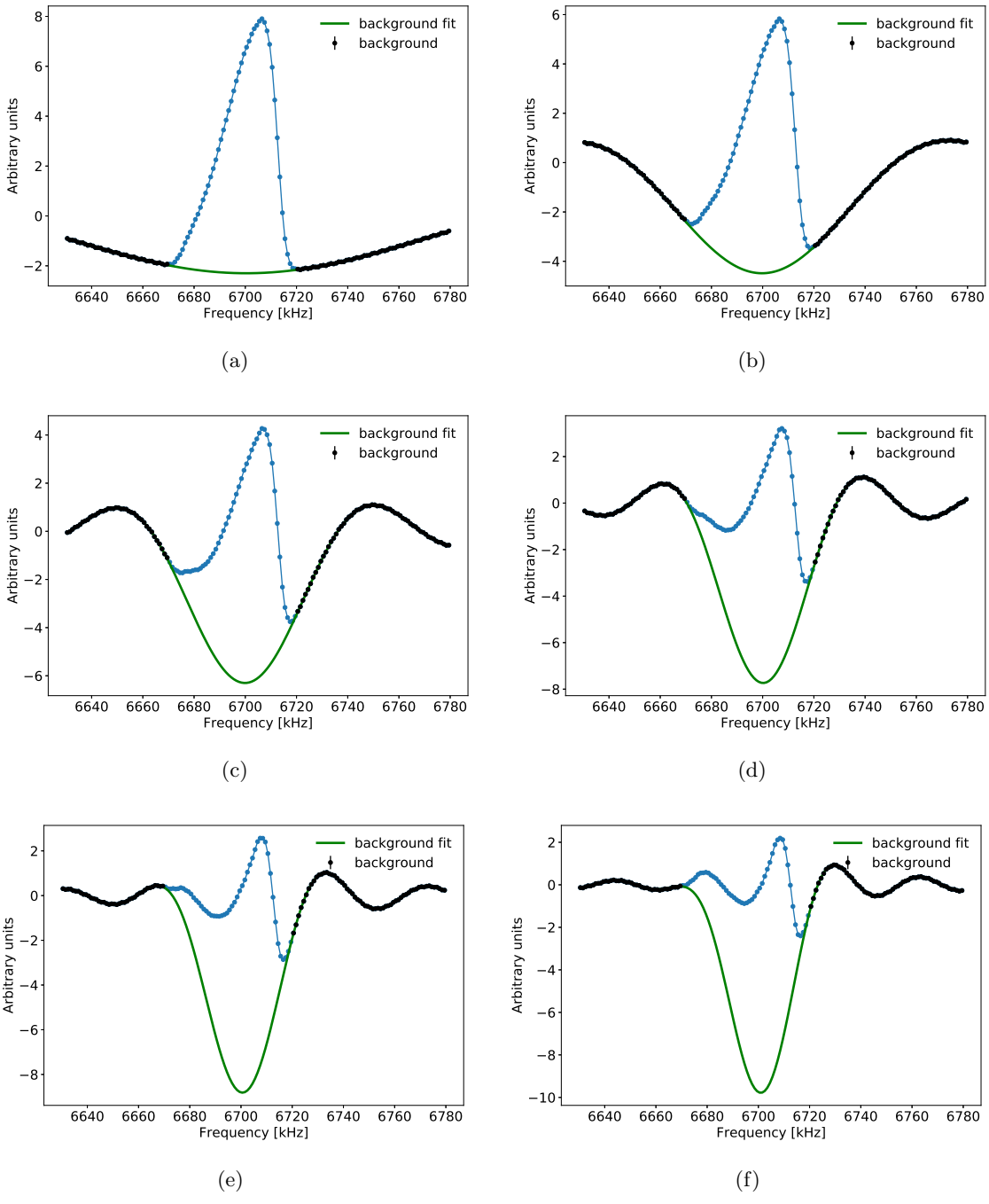

Figure 19: Background fit of the cosine Fourier transform for the TMC #3 using the triangle-based function:(a) $t_s = 5\ \mu s$, (b) $t_s = 10\ \mu s$, (c) $t_s = 15\ \mu s$, (d) $t_s = 20\ \mu s$, (e) $t_s = 25\ \mu s$, and (f) $t_s = 30\ \mu s$.

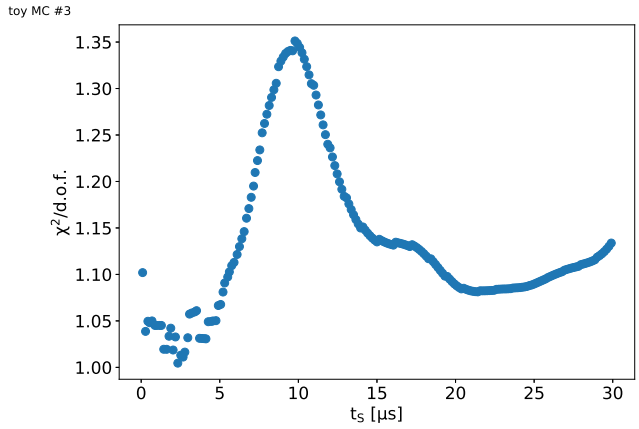

(a)

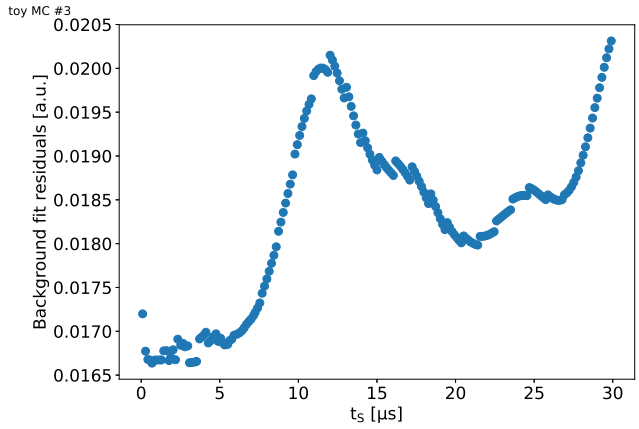

(b)

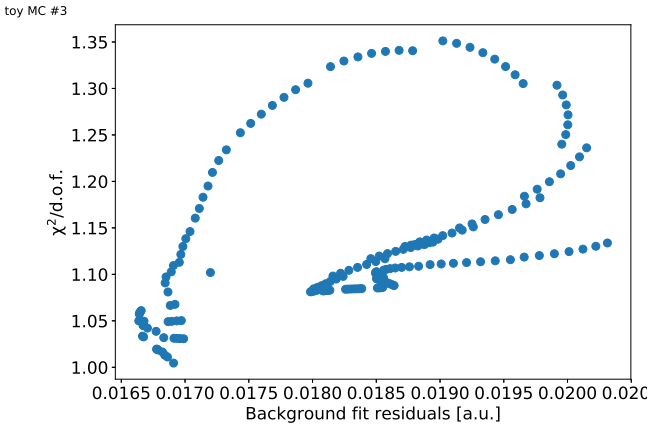

(c)

Figure 20: Background fit information for the triangle-based function for the TMC #3: (a) χ^2/d.o.f. as a function of t_s, (b) fit residuals as a function of t_s, and (c) χ^2/d.o.f. as a function of fit residuals.

4.3 t_m systematic

As explained in [1] Sec. 7.3, there is a trade-off increasing the length of the fast rotation signal between improving the resolution and adding increasing noise. The toy Monte Carlo simulations, un-like the data, do not have the increasing statistical noise with increasing t_m. The interest of performing a t_m scan is to gauge the minimal length of the fast rotation signal required to reach convergence once the resolution is high enough. Figures 21 and 22 show the t_m scans for respectively the TMC #1 and #3. The start time is set to $t_s = 4$ μs and the t_0 value, obtained via the cardinal sine optimization, is optimized for each value of t_m. It appears clear that the results converge for t_m values greater than 100 μs, i.e., 4-100 μs is the minimal time window required to have a high enough resolution. The results are very stable passed 100 μs. Though the resolution keeps increasing by adding more data point to the fast rotation signal, the beam is fully de-bunched and therefore the Fourier transform does not benefit from these extra data point. In the data, t_m will have to be chosen greater than 100 μs but smaller than an optimized value (typically 300, 400 μs) to avoid a performance reduction due to the increasing statistical noise at large t_m. The systematic uncertainty in the data will be estimated taking half the maximum variation observed in the scan results for a stable t_m range.

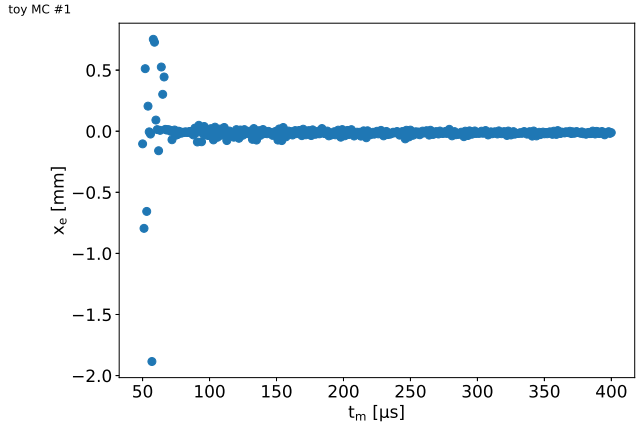

(a)

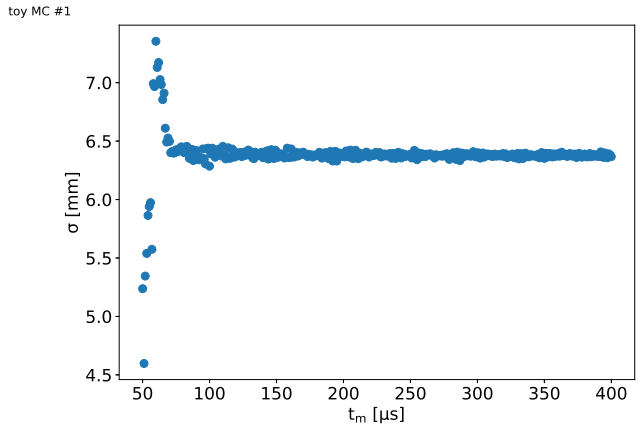

(b)

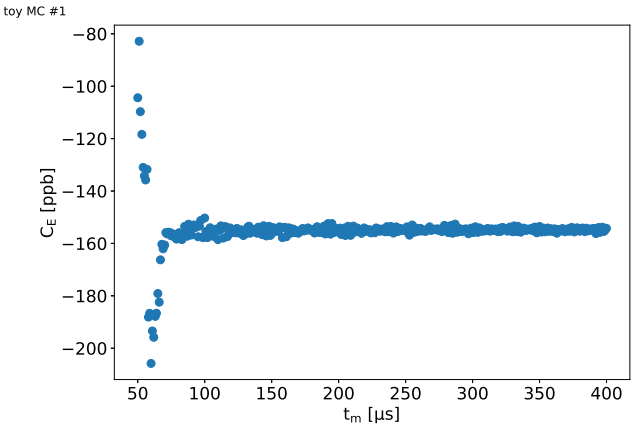

(c)

Figure 21: Results of the fast rotation analysis for $t_s = 4$ μs as a function of t_m for the TMC #1: (a) equilibrium radius, (b) width, and (c) electric field correction C_E. The known answers are (a) $x_e = -0.01$, (b) $\sigma = 6.40$ mm, and (c) $C_E = -156$ ppb.

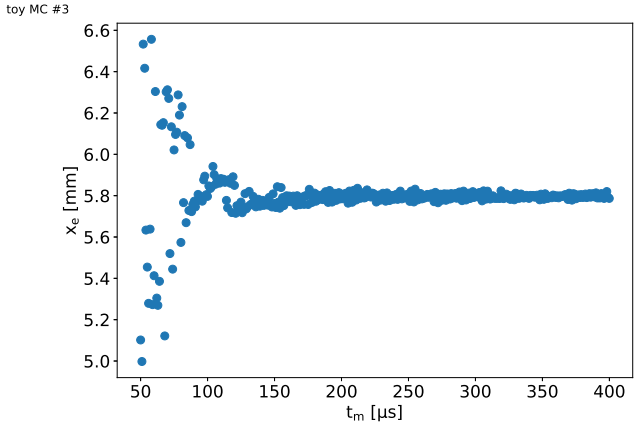

(a)

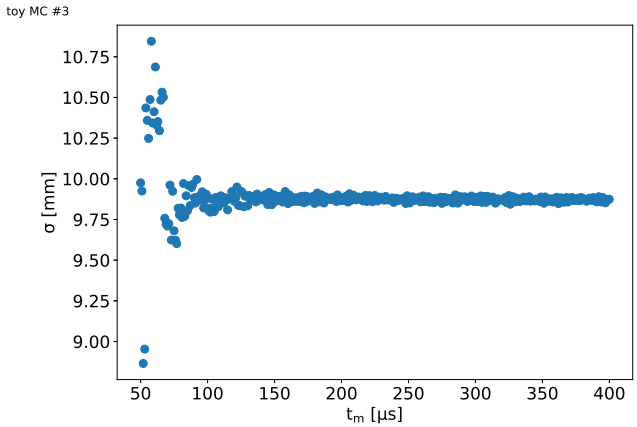

(b)

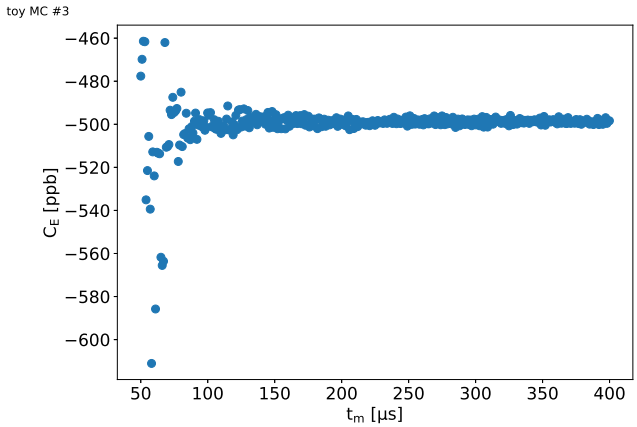

(c)

Figure 22: Results of the fast rotation analysis for $t_s = 4$ μs as a function of t_m for the TMC #3: (a) equilibrium radius, (b) width, and (c) electric field correction C_E. The known answers are: (a) $x_e = 5.80$ mm, (b) $\sigma = 9.87$ mm, and (c) $C_E = -499$ ppb.

4.4 Frequency interval

The nominal frequency interval used to compute the cosine Fourier transform is 1 kHz in the simulation and 2 kHz in the data (less statistics available in the data). As explained in [1] Sec. 7.3, this leads to over-sampling because the frequency resolution for a fast rotation signal starting at $t_s = 4\ \mu s$ and ending at $t_m = 300\ \mu s$ with a time interval of 1 ns is 3.4 kHz. In order to verify that the over-sampling does not lead to a systematic bias, a scan of the frequency interval is performed. The allowed values for the frequency interval are integer numbers of the frequency window used for the cosine Fourier transform. For instance, the nominal frequency window is 150 kHz wide, and for a 2 kHz frequency interval it leads to 75 bins. Choosing for instance 1.75 kHz for the frequency interval would yield a non-integer number of bins for the cosine Fourier transform if the frequency window remains 150 kHz. Figures 23 and 24 show the results of the frequency interval scans for the TMC #1 and #3. It appears that over-sampling is a necessity. This is due to the fact that the typical width of the frequency distribution is 5-10 kHz. To properly recover such width, the frequency sampling should be at least half the value of the width (Nyquist–Shannon sampling theorem). The systematic uncertainty in the data will be estimated taking half the maximum variation for the results with frequency intervals below 3 kHz.

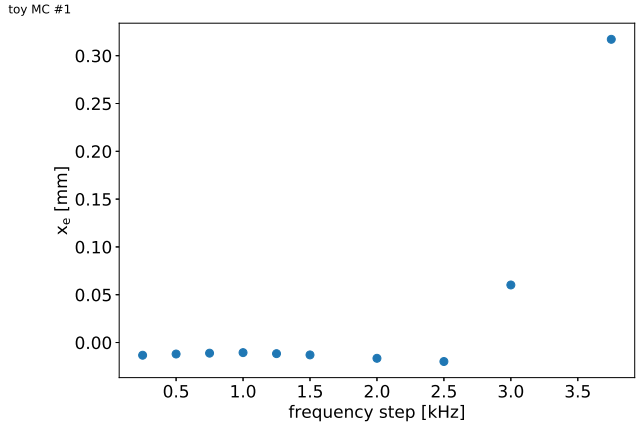

(a)

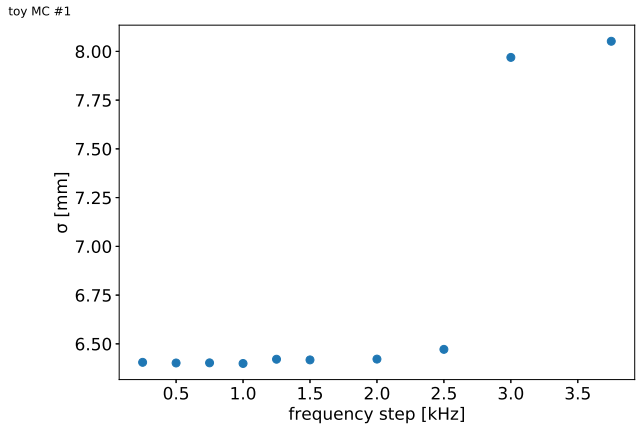

(b)

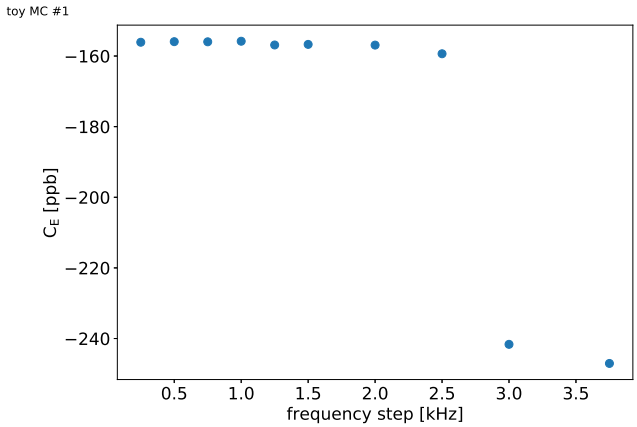

(c)

Figure 23: Results of the fast rotation analysis as a function of the frequency interval for the TMC #1: (a) equilibrium radius, (b) width, and (c) electric field correction C_E. The known answers are (a) $x_e = -0.01$, (b) $\sigma = 6.40$ mm, and (c) $C_E = -156$ ppb.

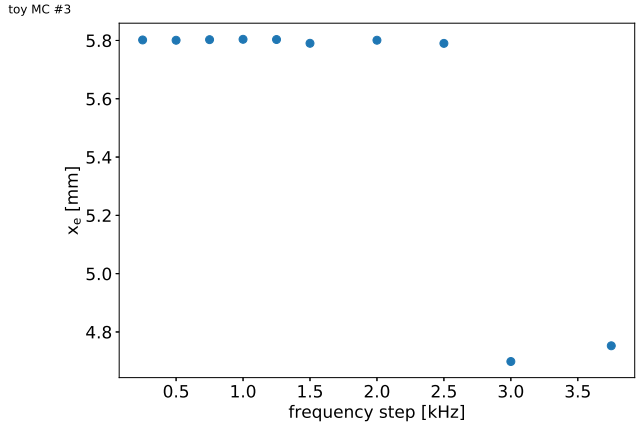

(a)

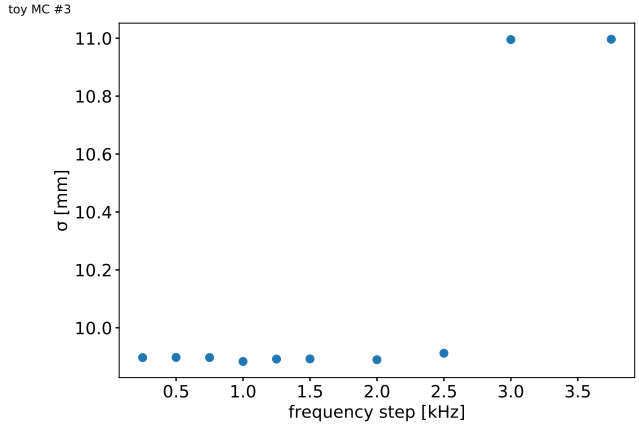

(b)

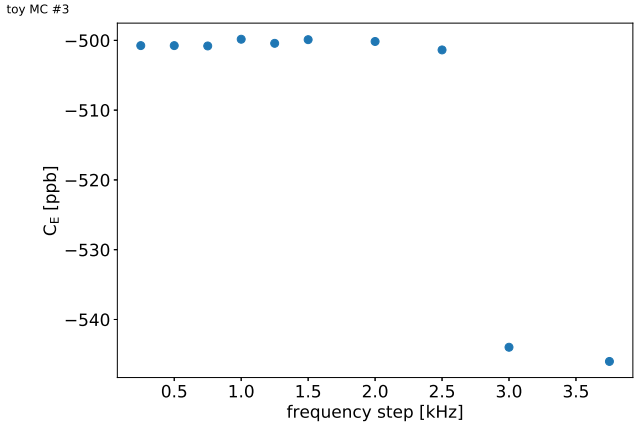

(c)

Figure 24: Results of the fast rotation analysis as a function of the frequency interval for the TMC #3: (a) equilibrium radius, (b) width, and (c) electric field correction C_E. The known answers are: (a) $x_e = 5.80$ mm, (b) $\sigma = 9.87$ mm, and (c) $C_E = -499$ ppb.

4.5 Background

The definition of the background is key for optimizing t_0 and correcting the cosine Fourier transform. The functional form of the background is already part of the t_0 systematic uncertainty. The other sources of uncertainty from the background have to do with how it is defined, and how its statistical fluctuation can affect the analysis results via a lever arm effect, the data point being far from the mean of the distribution.

The background of the cosine Fourier transform is defined as the data point that are within $\pm N \cdot \sigma_{bkg}$ of the fit with σ_{bkg} being the statistical noise of the background estimated from the fit residuals for the optimal t_0 value. The parameter that can be varied is N with its nominal value being $N = 2$. The larger N the closer to the mean of the distribution the background will get. Figures 25 and 26 show the background fit for two values of N for respectively the TMC #1 and #3: $N = 1$ and $N = 5$. Figures 27 and 28 show the results of the background threshold scan. The main take away is that for values of $N > 2$ the width of the radial distribution is reconstructed more poorly (up to about 0.1 mm shift between $N = 1$ and $N = 5$). This motivates the default value to be $N = 2$. The systematic uncertainty in the data will be estimated taking half the maximum variation observed in the scan results.

For actual data[4], the statistical fluctuation in the tail (background) of the frequency/radial distribution can bias the extraction of the equilibrium radius and width given potentially a large lever arm effect. This effect is addressed by removing (zero-ing out) the background from the distribution. The data point within $\pm N \cdot \sigma_{bkg}$ of the fit function (i.e. the data point tagged "background") are removed. This is done for several values of N, meaning for different definitions of the background. Figures 29 and 30 show the radial distributions for the TMC #1 and #3 for two different values of N. Figures 31 and 32 show the results of the background removal scan. The systematic uncertainty in the data will be estimated taking half the maximum variation observed in the scan results.

[4]The typical number of positron entering the fast rotation histogram is 10^9 in the data and 10^{10} in the simulation.

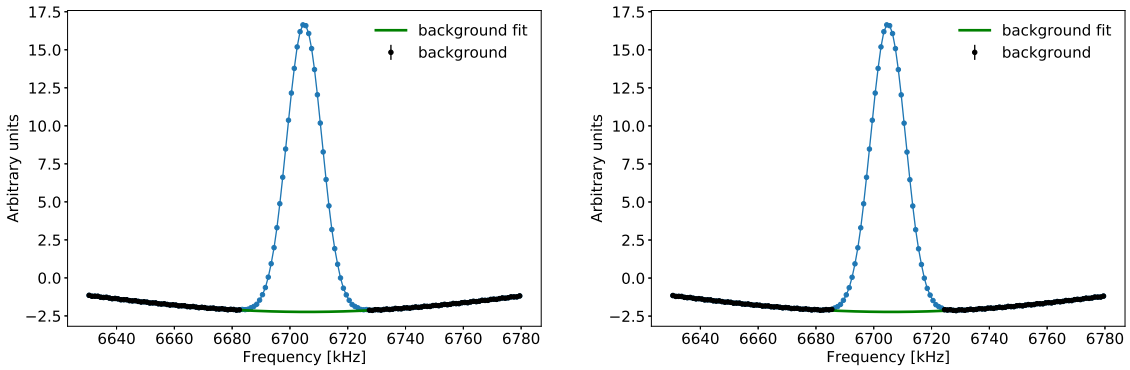

(a) (b)

Figure 25: Cardinal sine background fit of the cosine Fourier distribution for the TMC #1. The background threshold is (a) $N = 1$, and (b) $N = 5$.

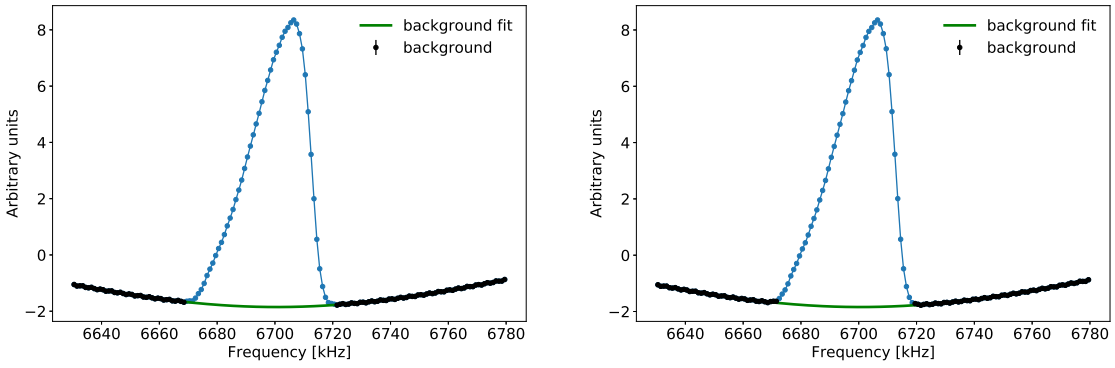

(a) (b)

Figure 26: Cardinal sine background fit of the cosine Fourier distribution for the TMC #3. The background threshold is (a) $N = 1$, and (b) $N = 5$.

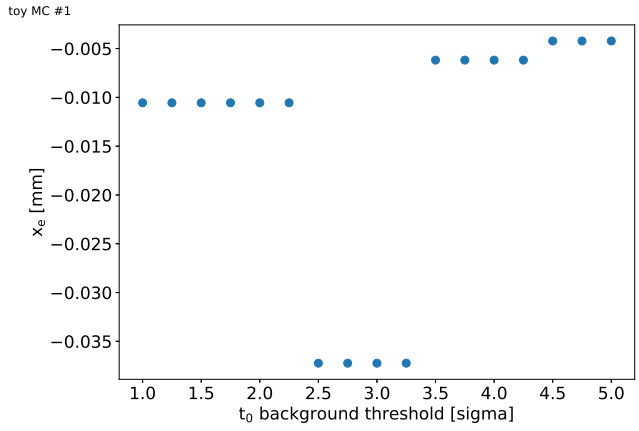

(a)

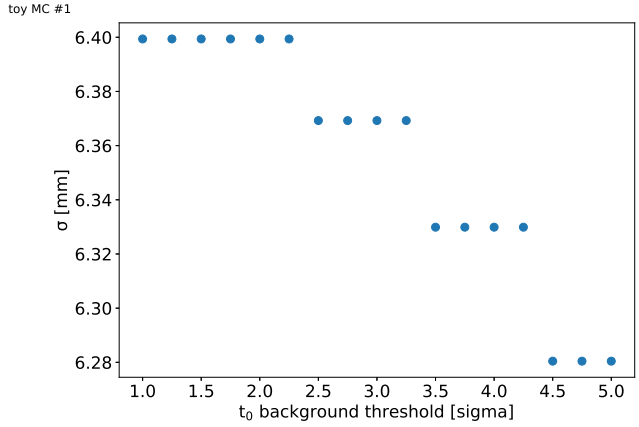

(b)

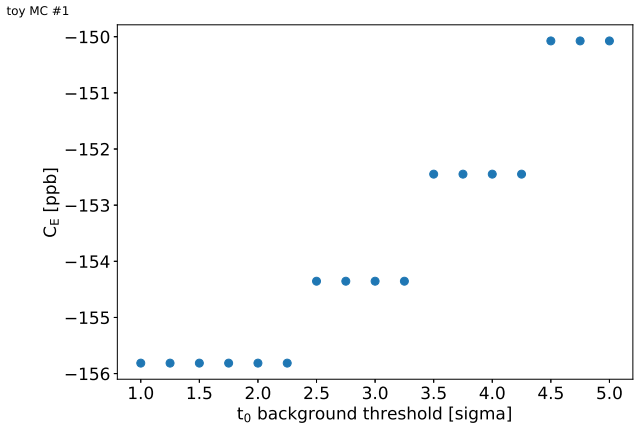

(c)

Figure 27: Results of the fast rotation analysis as a function of the background definition threshold N for the TMC #1: (a) equilibrium radius, (b) width, and (c) electric field correction C_E. The known answers are (a) $x_e = -0.01$, (b) $\sigma = 6.40$ mm, and (c) $C_E = -156$ ppb.

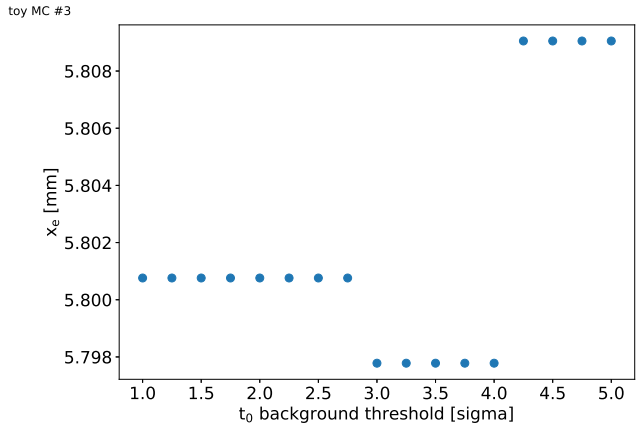

(a)

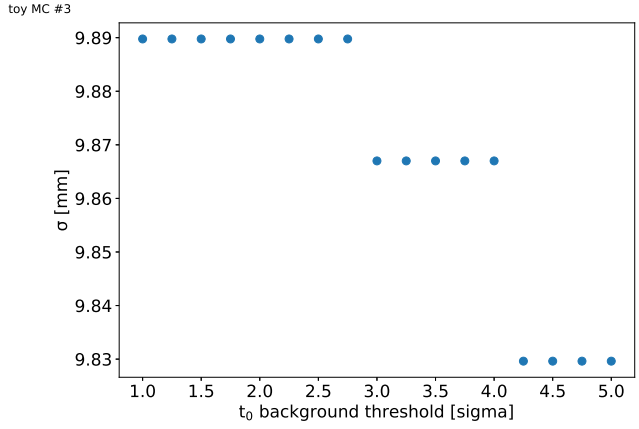

(b)

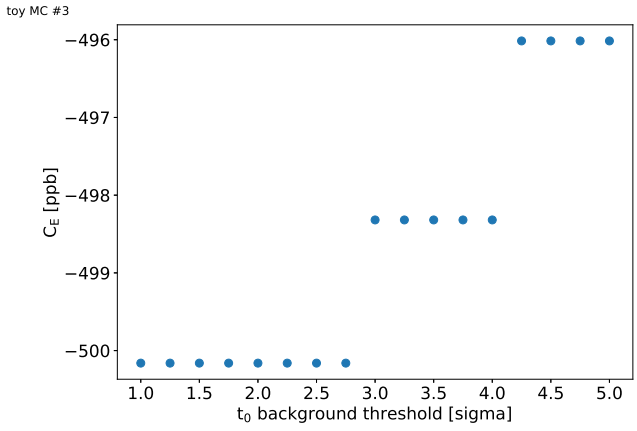

(c)

Figure 28: Results of the fast rotation analysis as a function of the background definition threshold N for the TMC #3: (a) equilibrium radius, (b) width, and (c) electric field correction C_E. The known answers are: (a) $x_e = 5.80$ mm, (b) $\sigma = 9.87$ mm, and (c) $C_E = -499$ ppb.

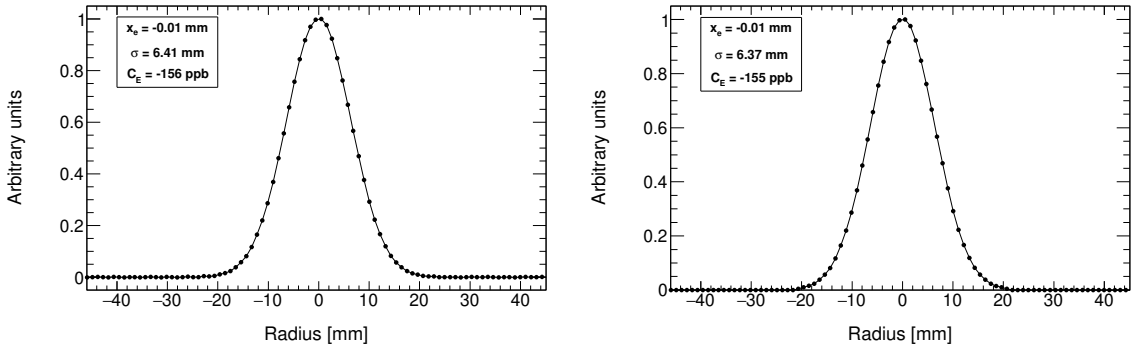

(a) (b)

Figure 29: Radial distribution for the TMC #1 for two N values with background removal: (a) $N = 1$, and (b) $N = 5$.

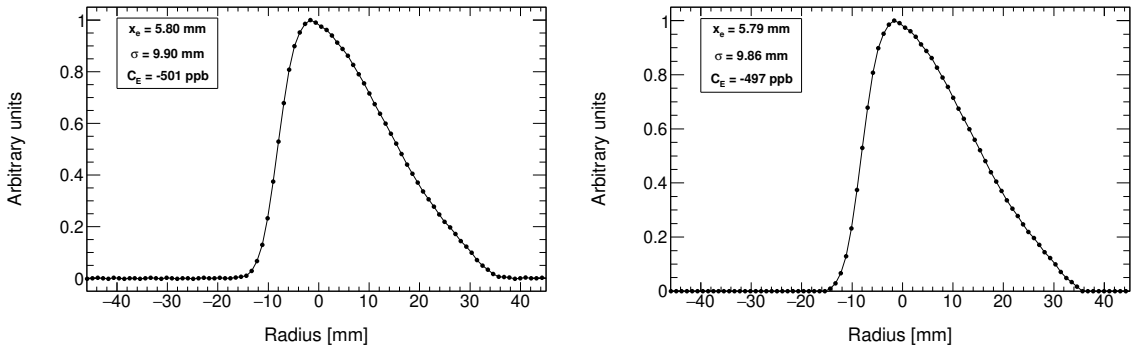

(a) (b)

Figure 30: Radial distribution for the TMC #3 for two N values with background removal: (a) $N = 1$, and (b) $N = 5$.

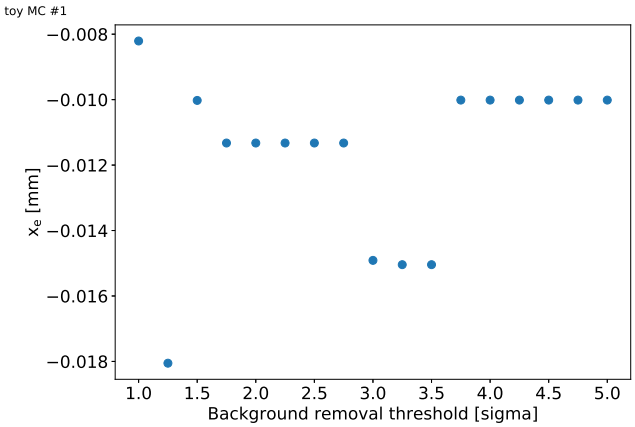

(a)

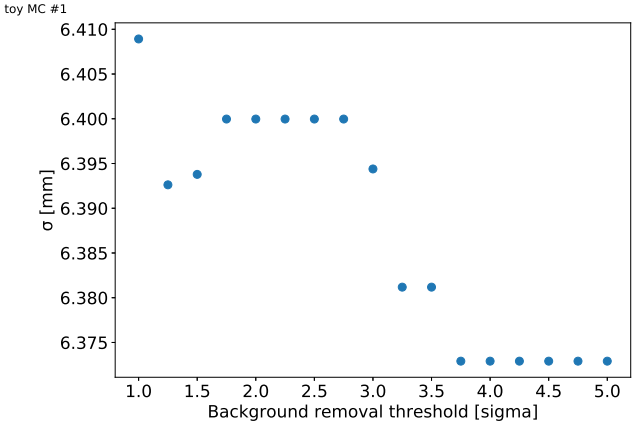

(b)

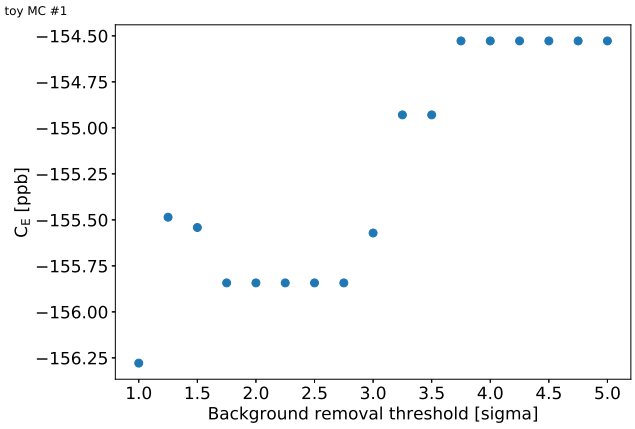

(c)

Figure 31: Results of the fast rotation analysis as a function of the background removal threshold N for the TMC #1: (a) equilibrium radius, (b) width, and (c) electric field correction C_E. The known answers are (a) $x_e = -0.01$, (b) $\sigma = 6.40$ mm, and (c) $C_E = -156$ ppb.

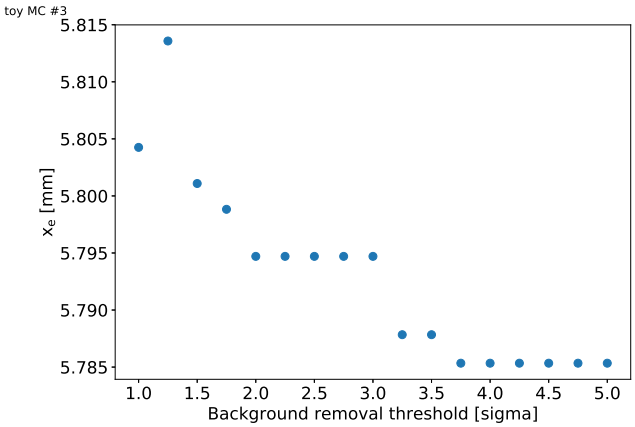

(a)

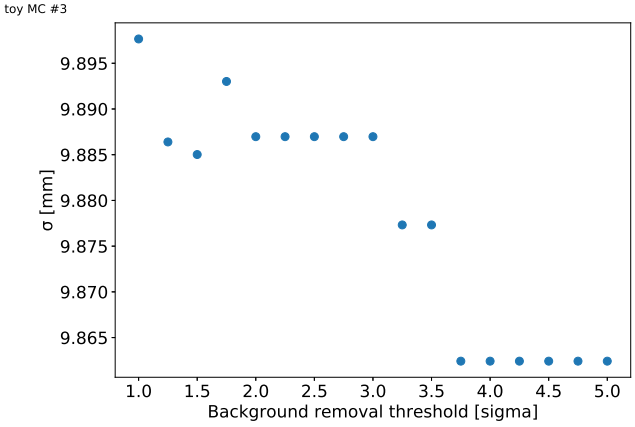

(b)

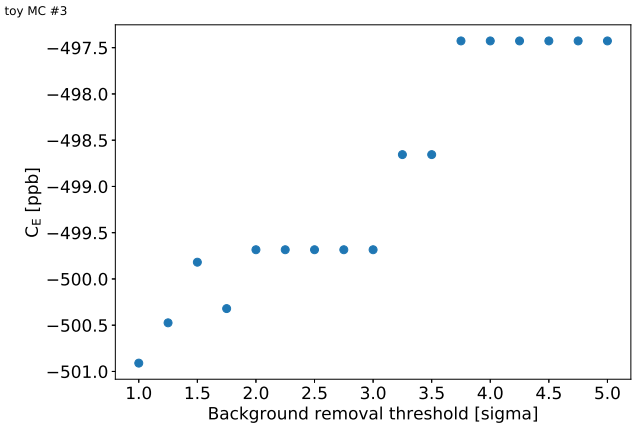

(c)

Figure 32: Results of the fast rotation analysis as a function of the background removal threshold N for the TMC #3: (a) equilibrium radius, (b) width, and (c) electric field correction C_E. The known answers are: (a) $x_e = 5.80$ mm, (b) $\sigma = 9.87$ mm and (c) $C_E = -499$ ppb.

5 Conclusion and outlook

This note showed that for fast rotation signals such as the TMC #1 and #3, the Cornell fast rotation Fourier method performs better than the desired goal of the Fermilab E–989 experiment. The foundation of the treatment of the systematic uncertainties has been laid down. The analysis of actual data will require estimating additional systematic uncertainties. This note did not discuss the effect of an asymmetric incoming longitudinal beam profile. The reason being that this is a non-issue: the method performs the same for symmetric and asymmetric beam profiles as motivated by the derivation in [10] Sec. 3.4. The TMC #2 [11] is an example of a fast rotation signals with an asymmetric beam profile. The analysis of the TMC #2 was not presented in this note because its beam profile peculiarity led to no noticeable difference in the method performance. Even though the good performance showed in this note, there is more work to be done using toy Monte Carlo simulations:

- study the effect of momentum-time correlation in the incoming beam, i.e., different time slices of the incoming beam have different momentum populations,
- study the effect of pile-up at early time in the fill,
- study the effect of gain change at early time in the fill,
- study the effect of muon loss if there exists a momentum-lost time correlation,
- study the effect of scrapping given it changes the closed orbit of the beam at early time.

These effects are suspected to be small from analyzing Run–1 data. Nonetheless these effects should be thoroughly studied with toy Monte Carlo to quantify their impact. Toy Monte Carlo simulation is a great tool to understand the performance of the fast rotation analysis. It is limited though in that it does not have the various complicated beam dynamics effects that is observed in the data. The next step to study the performance of the analysis is to use high-statistics simulations from `BMAD` and `GM2RINGSIM`. Such studies have started with BMAD but will not be the subject of a note for lack of time and people leaving the Cornell group. Hopefully a new effort can start using both `BMAD` and `GM2RINGSIM` to complete the performance study and allow a better estimation of the systematic uncertainties of analyzed data.

The Cornell fast rotation Fourier analysis is one implementation of the fast rotation Fourier analysis and there is room to try new ideas and come up with different approaches. The key point of the Fourier analysis is to deal with correcting the cosine Fourier transform given the missing early data. Thorough details and ideas can be found in [5][5].

[5] One idea not developed in [5] is the possibility of using the information from the sine Fourier transform. Also, the validity of the original equation for the background equation (correction term: see [10] Sec. 3.7.) was not discussed. It could be that this equation is only a good approximation.

References

[1] A. Chapelain, J. Fagin, D. Rubin, D. Seleznev, *Cornell fast rotation Fourier method*, GM2-doc-18901

[2] A. Chapelain, J. Fagin, D. Rubin, D. Seleznev, *Cornell fast rotation Fourier analysis user guide*, GM2-doc-18460

[3] See 'TMC #1' in: GM2-doc-13759

[4] See 'TMC #3' in: GM2-doc-13759

[5] A. Chapelain, J. Fagin, D. Rubin, D. Seleznev, *On the background correction of the Cornell fast rotation Fourier method*, GM2-doc-19225

[6] A. Chapelain, J. Fagin, D. Rubin, D. Seleznev, *Fast rotation analysis of the Run–1 60–hour data set with the Cornell Fourier method*, GM2-doc-19150

[7] A. Chapelain, J. Fagin, D. Rubin, D. Seleznev, *Fast rotation analysis of the Run–1 9–day data set with the Cornell Fourier method*, GM2-doc-19252

[8] A. Chapelain, J. Fagin, D. Rubin, D. Seleznev, *Fast rotation analysis of the Run–1 End-game game data set with the Cornell Fourier method*, GM2-doc-19258

[9] A. Chapelain, J. Fagin, D. Rubin, D. Seleznev, *Fast rotation analysis of the Run–1 High-kick data set with the Cornell Fourier method*, GM2-doc-COMING-SOON

[10] A. Chapelain, D. Rubin, D. Seleznev, *Extraction of the Muon Beam Frequency Distribution via the Fourier Analysis of the Fast Rotation Signal*, E989 note 130, GM2-doc-9701

[11] See 'TMC #2' in: GM2-doc-13759